J Nanostruct Chem (2015) 5:393–403
DOI 10.1007/s40097-015-0171-0

ORIGINAL RESEARCH

Nano-structured Mn–Al and Co–Al Oxide Materials for Catalytic Ethanol Conversion

Dalia R. Abd El-Hafiz[1] · M. Riad[1] · S. Mikhail[1]

Received: 3 June 2015 / Accepted: 31 July 2015 / Published online: 23 October 2015

Abstract Nano-sized mixed oxides of Manganese–aluminum and/ or cobalt–aluminum materials were prepared via co-precipitation method in basic medium associated with ultrasonic radiation to be used as catalysts for ethanol conversion reactions. The prepared materials were physically characterized via different technique. The results established the formation of spinel structure containing Co–Al oxides, while, plate and rod structures for that containing Mn–Al mixed oxides. Acetone is the main converted product at all reaction temperature on the two samples. On using Co–Al sample, the selectivity towards acetone formation reached the maximum value of ~85 % at 200 °C and decreased on increasing the reaction temperature to 500 °C in parallel with the increase in ethylene formation. Mn–Al mixed oxide shows a gradual increase in the selectivity towards the formation of acetone with the increase in reaction temperature (reached ~95 % at 500 °C).

Keywords Mn–Al · Coal · Nano-particles · Mixed oxide · Ethanol · Acetone

Introduction

The transformation of ethanol into valuable chemicals is of great interest in different countries owing to its huge production. As well known, the oxidative ethanol products are; acetaldehyde, ethylene, acetone, ethyl acetate and/or acetic acid [1, 2].

✉ Dalia R. Abd El-Hafiz
dalia_epri@yahoo.com

[1] Egyptian Petroleum Research Institute (EPRI), Cairo, Egypt

Noble metals (Rh, Ru, Pt, and Pd)-supported materials are very active catalysts for ethanol conversion, but the high cost of these materials limits their application [3]. Different catalysts, including transition metal oxides: Fe_2O_3–ZnO [4], or Fe_2O_3–CaO–MgO [5] are able to catalyze ethanol reaction at high reaction temperature which leads to the formation of undesirable byproducts and catalyst deactivation.

New active catalytic systems in which the formation of highly dispersed metallic species is favored are found to be active at lower reaction temperatures. Nishiguchi et al. [6] investigated steam reforming of ethanol over CuO/CeO_2, acetaldehyde and hydrogen were mainly produced at 260 °C and at 380 °C, acetone was the main product. The addition of MgO to CuO/CeO_2 promoted the ethanol conversion at lower temperature.

Rybak et al. [7] studied the conversion of ethanol on supported ceria, zirconia and ceria–zirconia cobalt oxide catalysts at reaction temperature 500 °C in a fixed-bed reactor. All catalysts exhibited high selectivity towards hydrogen and acetone formations. Sun et al. [8] studied the ethanol steam reforming on Co–ZrO_2 catalyst and found that the CoO and the basic sites are the most effective sites for acetone formation.

As known, the conventional Al_2O_3 and SiO_2 catalytic supports were used in the industry due to its acidic properties, high surface area and relatively low cost [9]. However, the acidic character of alumina may promote the ethanol dehydration reaction, producing ethylene, which can lead to high carbon deposition rates. So, ZrO_2 [10], CeO_2 [11], MgO [12] oxide materials have been recently studied as promising substituents for the conventional supports.

The current work is concerned with the preparation of the nano-structured (Mn–Al and Co–Al) mixed oxide

materials to achieve the complete and the selective ethanol conversion to be economically acceptable (low costs and low reaction temperature).

Experimental

Preparation of metal mixed oxides

Mn–Al and Co–Al mixed oxide materials were prepared by dissolving $Al(NO_3)_3{\cdot}9H_2O$ and $Mn(NO_3)_2{\cdot}4H_2O$, and/or $Co(NO_3)_2{\cdot}6H_2O$, salts with equal molar ratio (i.e., 1:1 Mn: Al or Co: Al) in distilled water. The co-precipitation was occurred by adjusting the pH of the solution to be 9.5 with the continuous drop-wise addition of the ammonia solution. The resulting solution was attained to sonication (Xin-Zhi, JY92-2D, Ti-horn, a power of 150 W and a frequency of 24 kHz) at an ambient temperature and for 90 min with a high-density ultrasonic probe immersed directly in the solution. The obtained precipitates were separated from the solution by centrifugation, washed with distilled water for several times until ammonia free, and dried at 120 °C. Then, the products were calcined in a flow of purified air with a heating rate of 10 °C min^{-1}, and kept at 450 °C for 4 h.

Structural phase changes

Different techniques were applied to investigate the physico-chemical characteristics of the prepared mixed oxides such as *X-ray powder diffraction analysis (XRD)*, and were carried out using a Shimadzu XD-1 diffractometer using Cu K_α radiation ($\lambda = 0.1542$ nm) at a beam voltage of 40 kV and 40 mA beam current. The intensity data were collected at 25 °C in a 2θ range of 4–80° with a scan rate of 0.7° s^{-1}. The Joint Committee on Powder Diffraction Society (JCPDS) database was used to index the peaks of XRD. *Thermal analysis* was performed to study the structural changes of the prepared materials with thermal treatment on SDTQ-600 (TGA-USA) thermo balance instrument. 10 mg of sample was heated up to 1100 °C, with a heating rate of 10 °C min^{-1} in an air flow at a rate of 100 ml min^{-1}. *Dynamic light scattering* (DLS) was performed to verify the particle size distribution of samples using Zetasizer Nano-ZS 90 (Malvern Instruments) operating at 600 nm and 90°. *High-resolution transmission electron microscopy* (HRTEM) and energy dispersive X-ray (EDS) were conducted using a JEOL 2100F TEM at an accelerating voltage of 200 kV. *Nitrogen adsorption/desorption isotherms*, BET surface areas, total pore volumes and average pore diameter were determined from the corresponding N_2 adsorption/desorption isotherms measured at −196 °C using a NOVA 3200 Unit, USA apparatus.

Catalytic activity

The catalytic conversion of ethanol was performed in a continuous fixed-bed flow system working under atmospheric pressure at the reaction temperature range 200–500 °C and at a space velocity 0.6 h^{-1} using N_2 as carrier gas with a flow rate of 40 ml min^{-1}. 0.5 g of the prepared material diluted with the quartz particles of the same size. Prior to the catalytic reaction, the prepared Co–Al and Mn–Al oxide materials were activated at 400 °C for 2 h, the ethanol was fed into the reactor with a flow rate of 0.2 ml h^{-1}. The products are subjected to gas chromatographic analysis using a Perkin-Elmer gas chromatograph with the flame ionization detector.

Results and discussions

X-ray diffraction analysis

X-ray diffraction pattern for the co-precipitated Co–Al and Mn–Al species and the related mixed metal oxide forms are depicted in Figs. 1 and 2.

The diffractogram for the co-precipitated Co–Al hydroxides (Fig. 1a) reveals the presence of low intensity and broad diffraction lines at: 10.3, 20, 34, 37, 60.5 and 63.5° which characterized the layer-structured Co–Al, a hydrotalcite-like phase [13], implying the poor crystallinity, and the dimensionality of the crystal size was in nanoscale. As known, layered double hydroxides consist of di- and trivalent cations; indeed, the presence of trivalent cations implies that the sheets are positively charged; the electrical neutrality of the compound was stabilized by the distributed anions between the hydroxylated sheets in the

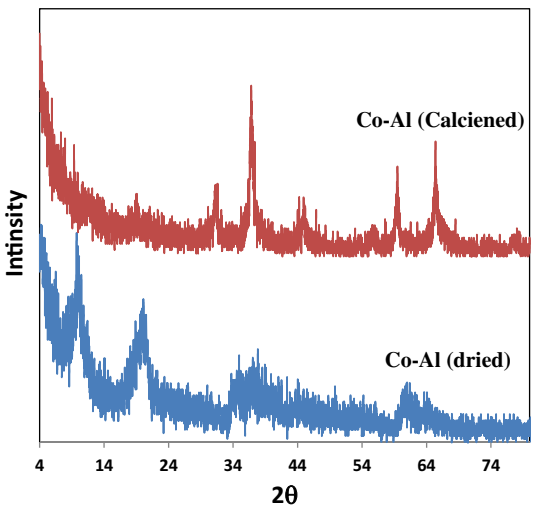

Fig. 1 XRD pattern of Co–Al samples

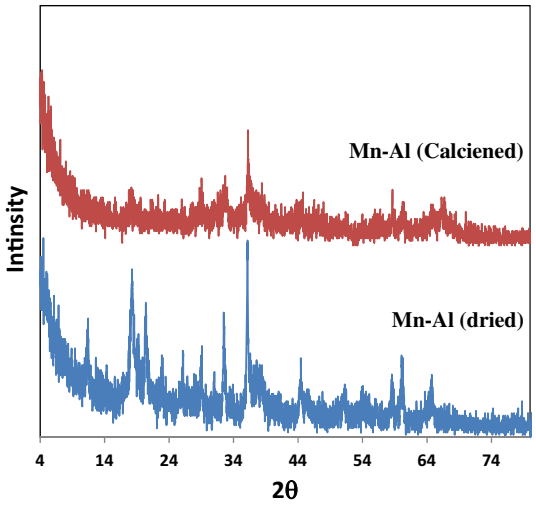

Fig. 2 XRD pattern of Mn–Al samples

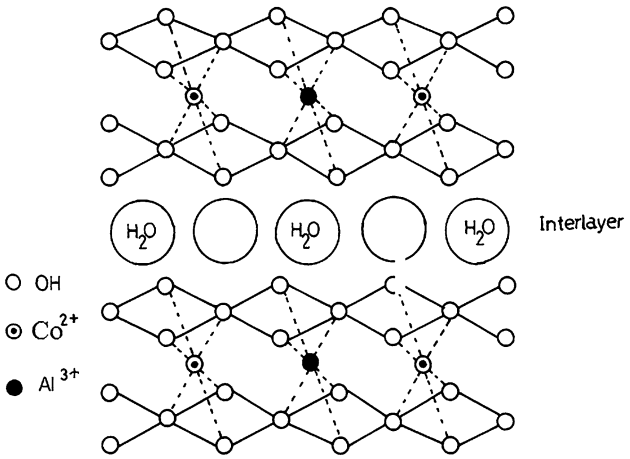

Scheme 1 Sketch for Co–Al LDH structure

disordered inter-lamellar domains, and the containing water molecules [14]. In this study, the ultrasonic radiation may promote the dissociation of water molecules, favoring the stabilization of the formed layers (as shown in Scheme 1), in agreement with Chang et al. [15] who postulated that the application of ultrasound in the preparation process promotes the formation of the hydrotalcite-like phase.

X-ray diffraction pattern for the calcined Co–Al material (Fig. 1b) detects diffraction lines at 2θ: 21, 31, 36, 45, 55, 59 and 65° to be indexed to spinel structures Co_2AlO_4, (JCPDS 38-0814); $CoAl_2O_4$, (JCPDS 82-2246) and Co_3O_4, (JCPDS 74-2120). However, it is rather difficult to distinguish between these mixed oxide phases due to the similarity of the cubic spinel structure with almost of the same characteristic reflection angles. In agreement with Palomaresa et al. [13] who prepared mixed oxides derived from layered double hydroxides (LDHs) and Jiang et al. [16] who studied the preparation of Co_xMg_{3-x}/Al composite oxides by calcination of Co_xMg_{3-x}/Al hydrotalcites at 800 °C. The significant diffraction peaks (with 2θ around 31°, 36°,39°, 45°, 55°, 59° and 65° reflections) confirm the presence of cobalt-containing spinel-type complex metal oxide phases. No characteristic reflections corresponding to the pure Al_2O_3 phase are observed.

The cobalt aluminate may be formed through the diffusion of Co^{2+} ions into the Al_2O_3 support, where Co occupies tetrahedral positions and Al fills the octahedral lattice sites. Furthermore, a part of Co could be substituted by Al in the Co_3O_4 phase, and consequently a stable spinel-type of $Co(Co, Al)_2O_4$ phase generated in the calcined mixed oxide [17]. Otherwise, the high reaction temperatures (>550 °C) favor the formation of these spinel-type phase and their formation under the experimental temperature 450 °C seems to be unlikely. The sonication condition may be the reason for the formation of the spinel structure at the lowest temperature.

For co-precipitated Mn–Al hydroxides, the diffraction pattern (Fig. 2a) detects sharp lines with a remarkable intensity at 2θ: 18, 20, 23, 26, 28.9, 31, 32.5, 36, 37.5, 38, 44.3, 45.2, 58.3, 60.5, 65° which indicate the formation of Mn_3O_4 species (JCPDS 24-0734). Diffraction lines for the formation of aluminum hydroxide or oxy-hydroxide are not detected.

XRD for Mn–Al mixed oxide (Fig. 2b) detects diffraction lines at 2θ: 18, 32.5, 38, 59°, which characterized the presence of Mn_2O_3 (JCPDS No. 41-1442). Another diffraction lines detected at 2θ: 38, 46.5, 67° are related to the formation of gamma-alumina crystal phase (JCPDS No. 10-0425). Even though the hydroxide form of aluminum is not detected, alumina diffraction lines are detected, this may be explained according to the following:

Mn species reacted with OH^- ions (strong base), a white insoluble $Al(OH)_3$ compound was obtained which may be coated by the precipitated manganese hydroxide due to the difference in the ionic radius.

The chemical reactions derived through sonication may be occurred in the following regions:

- The inner environment of the collapsing bubble (gas phase), where high temperatures and pressures are produced and causing the pyrolysis of water into H and OH radicals, and
- The interfacial region between the thin liquid shell surrounding the cavitation bubble and the bulk solution.

Concurrently, the reaction between the manganese hydroxide and the produced OH and/or H radicals (by the cavitation) takes place and a brown precipitate of $MnO(OH)_2$ was formed. Then, $MnO(OH)_2$ decomposed and Mn_3O_4 (Scheme 2) obtained [18, 19]. Upon calcination, Mn_3O_4 species is oxidized to Mn_2O_3 while the

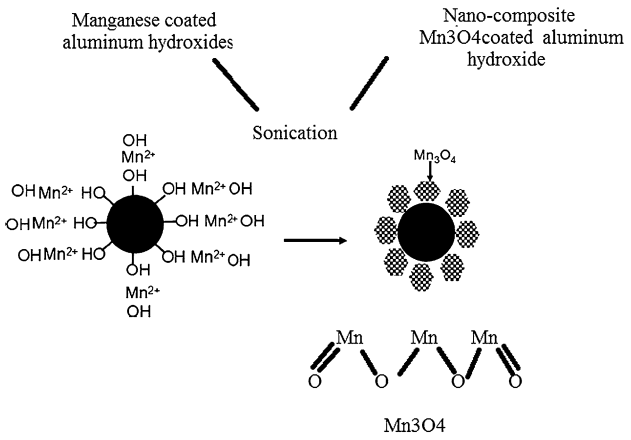

Scheme 2 Mn_3O_4 formation

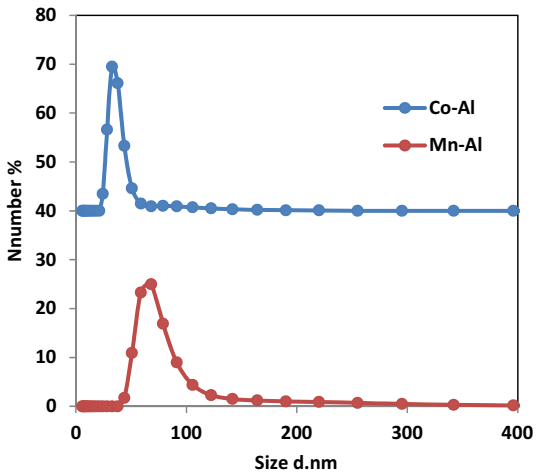

Fig. 3 Particle size distribution of the prepared samples

hydroxide form of the aluminum is liberated and oxidized to gamma alumina.

The low intensities and the broad diffraction peaks observed for the prepared Mn–Al and Co–A mixed oxide materials imply the poor crystallinity and the nanoscale dimension of the crystal size as confirmed by dynamic light scattering (DLS) (Fig. 3). Data in figure reveal that the particles for the two samples are in the nano-sized range (<100 nm). The measured average diameter for Co–Al is smaller than that for Mn–Al mixed oxide which may be attributed to the formation of $CoAl_2O_4$ spinel structure as confirmed by XRD data.

Table 1 shows the average atomic percentage of the mixed oxide as measured by EDX analysis, where it is proved that, the values of Mn, Co and Al in all regions are very close to the nominal composition of the mixed oxide suggesting that the preparation method leaded the required homogeneous distribution of the metals.

Table 1 Mixed oxide composition

Element	Weight (%)	Atomic (%)	Compd (%)	Formula
Co–Al				
Al K	17.6	19.12	33.26	Al_2O_3
Co K	52.49	26.1	66.74	Co_2O_3
O	29.91	54.78		
Mn–Al				
Al K	8.55	10.04	16.16	Al_2O_3
Mn K	64.93	37.45	83.84	MnO
O	26.52	52.51		

High-resolution transmission electron microscopy

TEM image for Co–Al mixed oxide sample (Fig. 4) shows congregates of nano-particles of cubic morphology characterize spinel cobalt oxide. In addition, the Co–O and Al–O bond energies are larger than that of Mn–O, which results in a stabilization of the Co spinel structure compared with that for Mn one.

TEM image for Mn–Al mixed oxide (Fig. 4) shows two distinct morphology, the first is a hexagonal plate structure which characterizes that gamma-alumina species are well dispersed on the external surfaces of the second structure which is a rod- or fiber-like morphology characterizing Mn–oxides species.

Thermal analysis

Differential and gravimetric thermal profiles for the prepared mixed oxide samples are depicted in Figs. (5, 6). The DTA profile for the prepared Co–Al reveals the appearance of three endothermic peaks at 96.5, 259.5 and 350 °C. The first is related to the removal of surface adsorbed water, meanwhile the second endothermic peak can be attributed to the complete loss of the intercalated water and partial loss of hydroxyl ions, and the last one reflects the formation of Co–Al mixed oxides. There are no changes noticeable from 800 to 1000 °C, indicating the high thermal stability of the prepared mixed oxide materials.

The TG profile revealed the thermal evolution, behavior of Co–Al mixed oxide. Three significant weight losses are observed within the temperature from 40 to 500 °C. It is well known that the first stage weight loss (8.8 % at 40–160 °C) is due to the release of the interlayer water. The second step of the weight loss that occurs (24.8 %) at 160–300 °C is due to the dehydroxylation of the interlayer hydroxyl groups with the evolution of H_2O. The last one (5.5 %) at 300–475 °C is related to the formation of Co–Al mixed oxide [20, 21].

The DTA profile of the prepared Mn–Al mixed oxide sample (Fig. 6) detects two endothermic and one

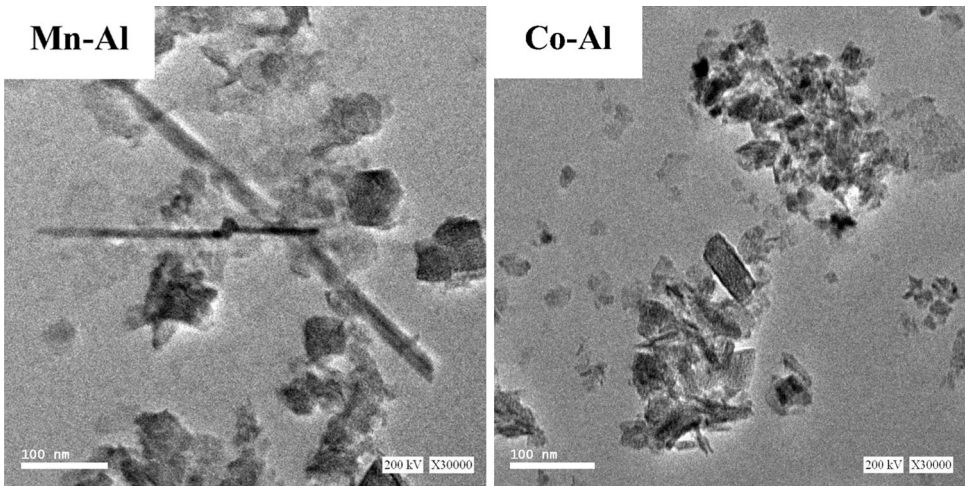

Fig. 4 Transmission electron microscope images of the prepared samples

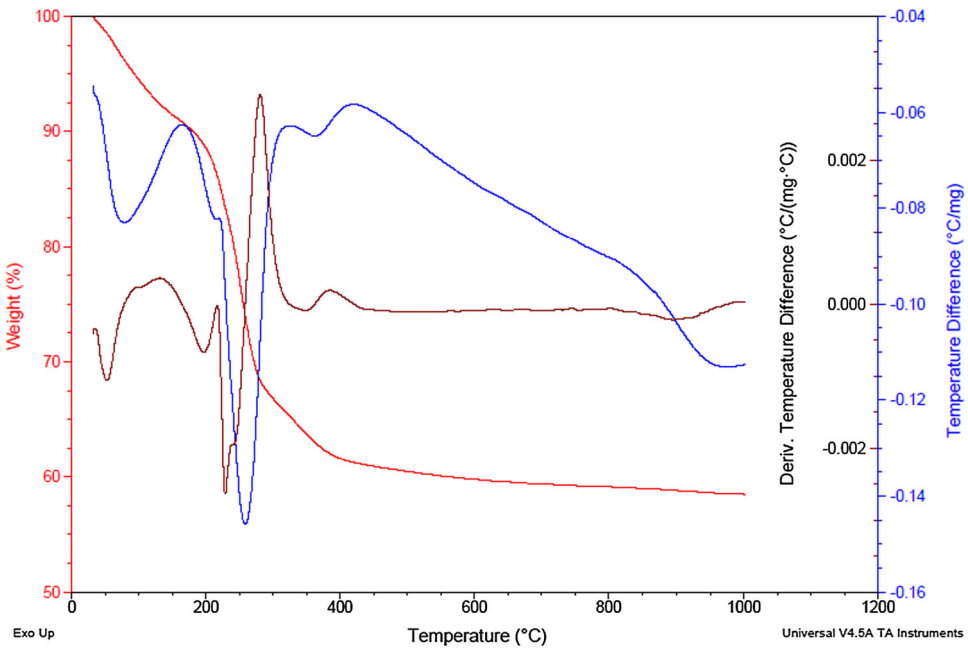

Fig. 5 Thermal gravimetric and differential thermal analysis of Co–Al

exothermic peaks. The endothermic peak appeared at ~75 °C which is related to the loss of the physisorbed water on the external surface of the mixed oxide material or in their pore channels. The second endothermic peak detected at ~275 °C is related to the oxidation of Mn_3O_4–Mn_2O_3 in addition to the elimination of water from the surface of the layered boehmite and its decomposition to gamma alumina (in agreement with XRD results). The exothermic peak detected at ~750 °C is related to the phase transformation of gamma to alpha alumina. The thermal events for the conversion of boehmite are habitually appeared at higher temperature (450–900 °C) [22]. This result reflects the important role of the ultrasound irradiation in the synthesis of Mn_3O_4 besides the enhancing effect in the transformation steps of boehmite to alpha alumina at lower temperature.

TG profile reveals three thermal weight loss steps, the first (6.6 %) occurred at the temperature range 40–170 °C which related to the removal of the physisorbed water. The second step (140–310 °C) is accompanied by a large weight loss (17.5 %) which related to oxygen liberation from Mn_3O_4 and its oxidation to Mn_2O_3 besides the decomposing of the boehmite to gamma alumina. The last weight loss (7.5 %) occurred at 310–860 °C is related to conversion of gamma to alpha alumina, in agreement with DTA results.

Surface texture measurements

The N_2 adsorption–desorption isotherms for the mixed oxide samples are shown in Fig. 7. The textural properties, including BET surface areas, average pore radius (r_P), and total pore volume (V_P), are listed in Table 2.

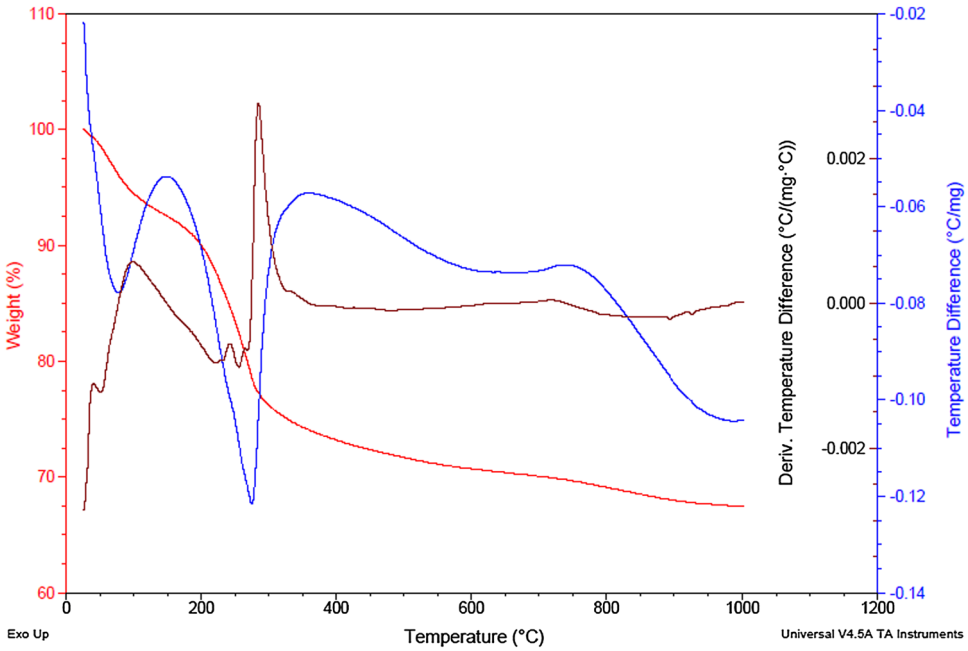

Fig. 6 Thermal gravimetric and differential thermal analysis of Mn–Al

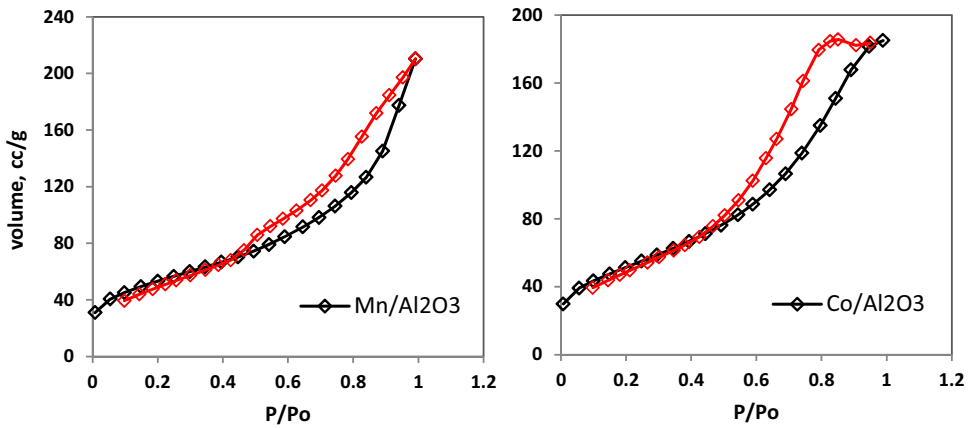

Fig. 7 N_2 adsorption–desorption isotherms for the prepared samples

Mn–Al mixed oxide (Fig. 7) exhibits type VI isotherms in accordance with the IUPAC classification corresponding to principally both micro- and mesopores with H3 type hysteresis loop characteristic of pore agglomerates in slit or plate form with non-uniform sizes. While, Co–Al mixed oxide exhibits isotherm of type IV with a distinct H2 type hysteresis loop, characteristic of solids whose pore structures are complex and tend to be made up of interconnected networks of pores of different size and shape [23]. Accordingly, the distribution and homogeneity of the pores are lower for this sample, and this can affect the catalytic activity for structure-sensitive reactions, in agreement with TEM results.

The inflection point or knee of the isotherm indicates the stage at which monolayer coverage is complete followed by multilayer adsorption. An initial increase adsorption capacity is observed for both samples, which are assigned to monolayer adsorption on the micropore surface as well as monolayer and initial multilayer adsorption in the mesopore intra wall at relatively lower pressures ($P/P_0 < 0.1$).

The S_{BET} for Co–Al and Mn–Al mixed oxide samples are nearly similar, (184.3 and 187 $m^2\ g^{-1}$, respectively). Meanwhile, micropores surface area for Mn–Al is higher (18.7) than that for Co–Al one (13 $m^2\ g^{-1}$). The results can be correlated with Co spinel-like phases segregated as evidenced by XRD, which may have relatively low surface areas, thus lowering the textural properties of Co containing mixed oxide. The Co–Al sample exhibits a lower pore volume, 0.31 cc g^{-1}, higher pore radius, 26 A° compared with Mn–Al mixed oxide 0.34, 19, respectively

The volume of gas adsorbed versus the statistical thickness, t of the physically adsorbed layer as a function

Table 2 Texture characteristics of the prepared sample

	BET method			*v-t* method			BJH method		
	S_{BET} (m^2 g^{-1})	V_p (cc g^{-1})	r_p (Å)	V_m (cc g^{-1})	S_{Micro}.(m^2 g^{-1})	S_{Ext} (m^2 g^{-1})	S_{BJH} (m^2 g^{-1})	V_p (cc g^{-1})	r_p (Å)
Co–Al_2O_3	184.3	0.29	31.0	0.011	13.1	171	223	0.31	26.8
Mn–Al_2O_3	187.0	0.33	34.8	0.008	18.7	168	213	0.34	19.6

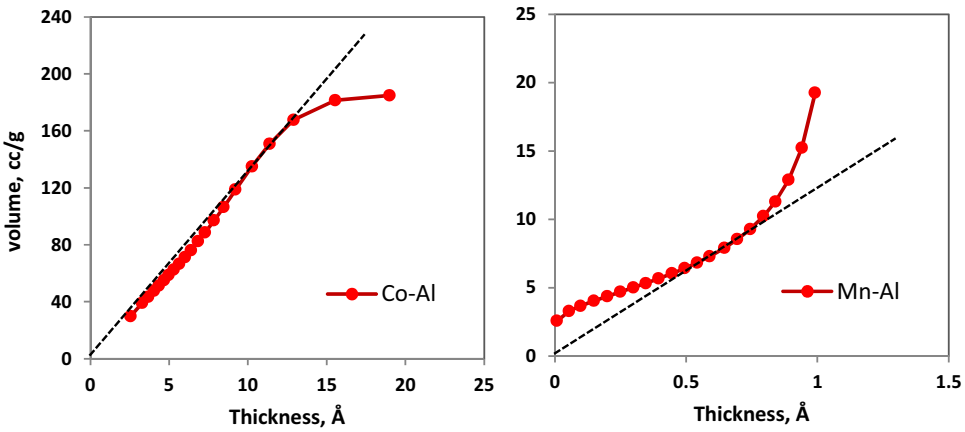

Fig. 8 *v–t plot* of the prepared samples

of relative pressure is used to shed light on pore nature. Three distinct linear stages are observed in the *t*-plots, initial stage of adsorption on the pore wall; intermediate stage of condensation; and last stage of adsorption on the external surface.

Mn–Al mixed oxide is mesoporous and is visualized from the upward deviation of the *t* plot start at $t \sim 0.75$ A°. The plot reveals low adsorbed volume at pore walls and mesopores but with unlimited adsorption at the external surface which reflects non-uniformity of pore structure, in agreement with TEM image.

Co–Al mixed oxide showed unexpected downward deviation (Fig. 8), i.e., microporous materials with a remarkable increase in volume (corresponds to the occurrence of capillary condensation in the mesopores) and thickness of adsorbed gas, but lower micropore surface area, total pore volume wide pore radius compared with Mn–Al mixed oxide. This reflects that, the interaction of aluminum species with cobalt one causes the creation of deep narrow micropores within the walls of the primary mesopores. This may form a three-dimensional channel system with connections between the mesopores, facilitating this observed amount of the adsorbed gas [24], and the predominance of microporosity in agreement with micropore volume (0.011 cc g^{-1}) compared with mesoporous Mn–Al (0.008 cc g^{-1}).

The pore size distribution of the prepared samples (Fig. 9) was determined using BJH method applied to the desorption branch. Bimodal distribution was observed for the two samples, Co–Al exhibits narrow pore size distributions in the mesopores range 5–85 nm: (centered at 20, 35 nm).

Mn–Al mixed oxide exhibits broad bimodal pore size distribution in the range 5–150 nm (The first is centered at 25 nm and the second at 55 nm in the mesopore range) compared with Co–Al mixed oxide, in agreement with *t* plot. This may be due to the diffusion of some alumina species inside manganese oxide ones resulting in the pore broadening (because the ionic radii of aluminum ions 0.535 nm are smaller than that of manganese 0.645 nm).

The pore structure configurates the presence of narrow pores for Co–Al mixed samples, probably indicating the formation of smaller particles size. Thus, Mn–Al mixed oxide exhibits wide bimodal mesoporous nature which favors reactant and product diffusion; one might expect that this dual porosity makes a mixed oxide superior candidate for catalytic reactions [25].

Catalytic activity

Total conversion and product distribution results from the reaction of ethanol conversion over the prepared mixed oxide sample (Mn–Al & Co–Al) catalysts at a temperature range (200–500 °C) are shown in Figs. (10, 11, 12, 13).

It was found that the total conversion increased continuously with increasing the reaction temperature on using the two prepared samples. The Co–Al showed better catalytic activity (total conversion ~ 100 %) than Mn–Al

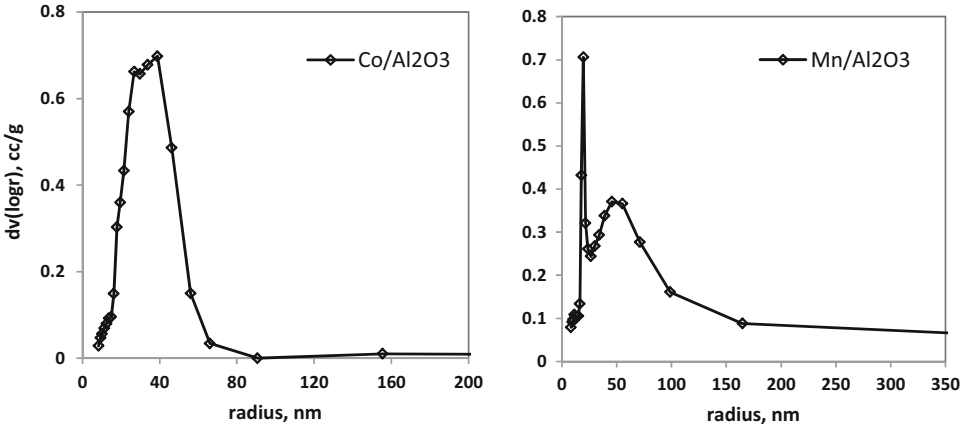

Fig. 9 Pore size distribution of the prepared samples

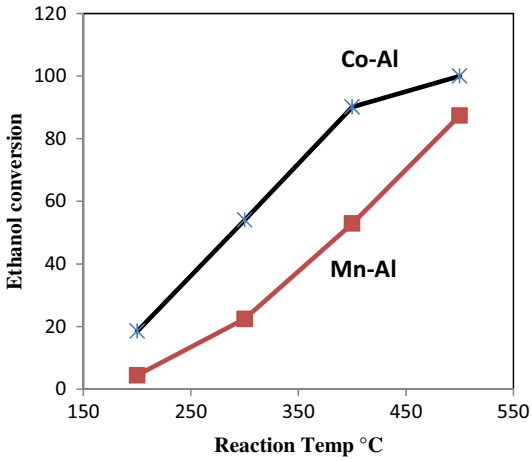

Fig. 10 Ethanol conversion over the prepared catalysts

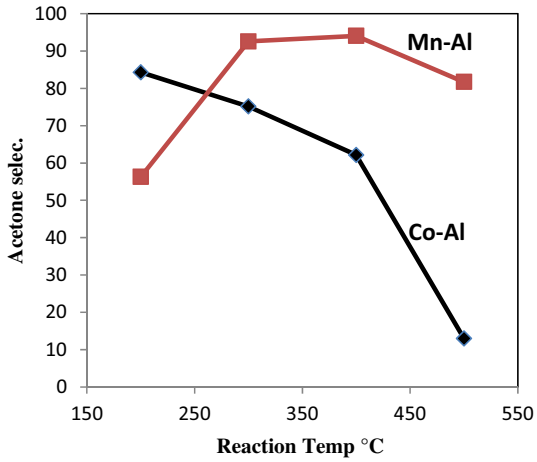

Fig. 11 The selectivity toward acetone formation over the prepared samples

(total conversion ~87 % at 500 °C), i.e., complete conversion of ethanol was achieved on Co–Al sample. This may be attributed to the comparable surface area of the two catalysts. It has been suggested that Al^{3+} ions polarize the covalent Co–O bonds in the spinel-like mixed oxide $Co(Co, Al)_2O_4$, (namely $Co^{2+}(Co^{3+}, Al^{3+})_2O_4$) resulting disturbed Co ions, which play as electron donor species; increasing the effective charge of the Co ions makes them more readily to donate electrons. Thus, facile one-electron transfer ensures the redox couple Co^{2+}/Co^{3+} and the anion vacancy close to Al^{3+} ion and consequently the high activity of the Co–Al sample [26].

Over the two samples (Table 3), reaction products were mainly composed of acetone, acetaldehyde, ethylene and trace amount of acetic acid and ethyl acetate. However, acetone has a low yield at reaction temperature 200 °C and increased sharply with a remarkable amount with the increase in the reaction temperature until reaching its maximum value 71.5 % at 500 °C with selectivity 81.7 % (Table 1) on using the prepared Mn–Al sample, in

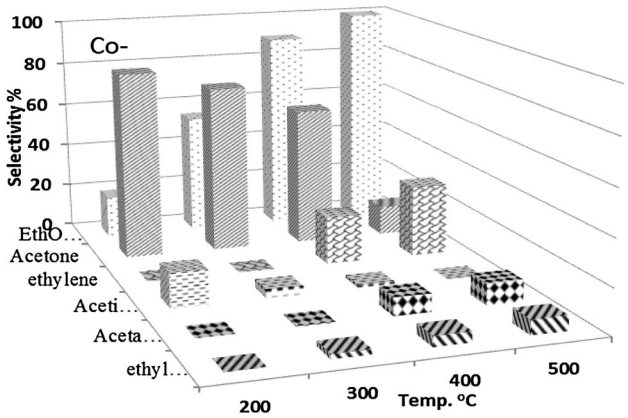

Fig. 12 The selectivity of the converted products over Co–Al samples at different reaction temperatures

agreement with the results of Rodrigues et al. [27]. The other products: acetaldehyde, ethylene and ethyl acetate were negligibly detected, while acetic acid appeared at

300 °C and increased sharply to reach ~13 % with the gradual increase in the reaction temperature to 500 °C. Meanwhile, on using the Co–Al, acetone formation was detected with an obvious amounts at 200 °C (15 %), then increased with the increase in reaction temperature successively to 400 °C until reaching a maximum value of 56 % and then decreased to 13 % at 500 °C, in parallel with the increase in the yield of ethylene. Moreover, acetaldehyde formation increased with the increase in reaction temperature and reached ~9 % at 500 °C.

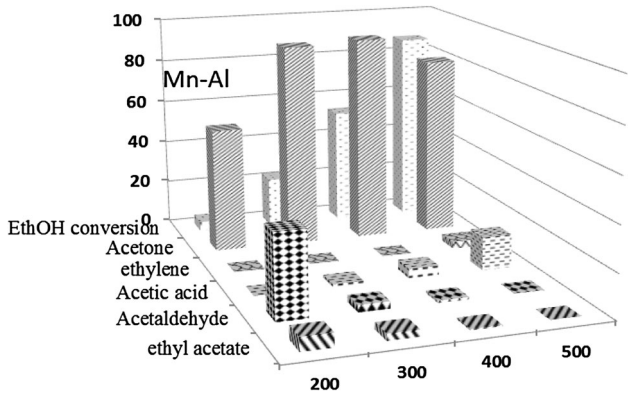

Fig. 13 The selectivity of the converted products over Mn–Al samples at different reaction temperatures

The prominent increase in acetone formation on Mn–Al along with the temperature increase in comparing with Co–Al sample (Fig. 11) may be attributed to the difference of the pore structure; the Mn–Al mixed oxide exhibits mesopore structure wider than that for the Co–Al one which allow the desorpated acetone through condensation/ketonization pathways to proceed easy without product diffusion hindering, as confirmed from surface texture results. Besides, the lattice defect resulting from the agglomerates of manganese oxides (has labile oxygen atoms) may participate in the acetone formation reaction.

The production of ethylene on Co–Al sample with remarkable amounts is accomplished on Brønsted acid sites. At higher reaction temperature, these sites may be formed during the diffusion of oxygen atoms from the spinel Co oxide, which becomes more significant and the reconstruction of the Co surface to form bounded hydroxyl groups with the assists of hydrogen rich in the reaction system [28]. Brønsted acid sites are supposed to represent the active sites in the reaction, and also inhibit the formation of byproducts, i.e., acetaldehyde and higher hydrocarbons.

On the other hand, it has been reported that the selectivity towards acetone formation was decreased by increasing the reaction temperature over Co–Al sample in consistence with the increase of acetaldehyde, ethylene and

Table 3 Effect of reaction temperature on the catalytic conversion of ethanol over the prepared Co–Al and Mn–Al samples

Temp (°C)	EtOH conversion	Acetaldehyde	Acetone	Acetic acid	Ethyl acetate	Ethylene
Conversion (mmol)						
Co–Alon						
200	18.45		15.55	2.80	0.00	0.00
300	53.96	0.22	40.53	2.00	1.18	0.00
400	90.13	7.19	56.01	1.32	4.10	19.20
500	100.00	9.57	12.99	0.00	6.54	31.98
Mn–Al_2O_3						
200	4.40	1.66	2.48	0.00	0.27	0.00
300	22.41	0.72	20.75	0.29	0.66	0.00
400	52.92	0.53	49.78	2.32	0.29	0.00
500	87.40	0.10	71.42	13.11	0.00	2.77
Selectivity (%)						
Co–Al_2O_3						
200		0.00	84.28	15.18	0.00	0.00
300		0.41	75.12	3.71	2.19	0.00
400		7.98	62.14	1.46	4.55	21.30
500		9.57	12.99	0.00	6.54	31.98
Mn–Al_2O_3						
200		37.64	56.30	0.00	6.07	0.00
300		3.20	92.58	1.28	2.95	0.00
400		1.00	94.07	4.39	0.54	0.00
500		0.11	81.71	15.00	0.00	3.17

ethyl acetate (Fig. 12). While, over Mn–Al sample, the acetone selectivity increases with the gradual increase in the reaction temperature (Fig. 13), accordingly, the selectivity towards acetaldehyde decreases. The acetone selectivity shows a maximum at 400 °C and then decreased in consistence with an increase in ethylene and acetic acid. This indicates that the acetone synthesis might occur on the metal surface and the two metals behave in a different catalytic manner with the gradual increasing in reaction temperatures.

Reaction mechanism

Ethanol was dehydrogenated first on basic sites to give acetaldehyde. Acetone is formed through two routes (Scheme 3):

- Acetaldehyde is oxidized to acetic acid, which is ketonized to acetone
- Or through Aldol condensation of acetaldehyde and then dehydrogenation and decarboxylation of the intermediate gives acetone.

So, the mechanism of conversion of ethanol to acetone over Mn–Al sample is performed via oxidation of acetaldehyde into acetic acid on metal oxide, which involved lattice oxygen abstraction leading to the formation of oxygen vacancies (Mn_2O_3), then acetic acid is ketonized to acetone, this mechanism is supported by detecting acetic acid in the reaction products.

The mechanism of formation of acetone on Co–Al sample may be performed via aldol condensation of acetaldehyde on basic sites (Co) to abstract hydrogen atom and strong Lewis acid sites (alumina) to bind the two molecules of acetaldehyde to form acetaldol, which dehydrogenated to 1,3 dicarbonyl, and then undergoes a cleavage that generates acetone [29, 30]. It is well known that the aldolization process is accompanied with a high amount of water released under reaction conditions.

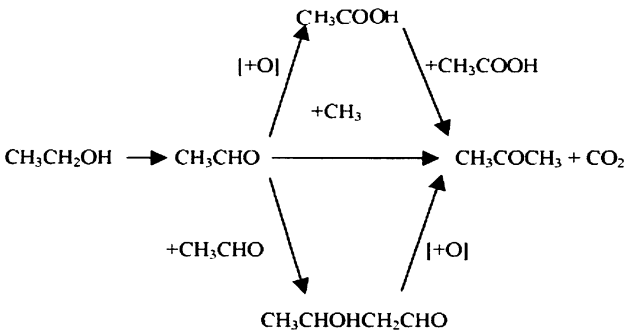

Scheme 3 Conversion of ethanol into acetone

Conclusion

From the previous results it can be concluded that:

- Nano-sized metal oxides Co–Al and Mn–Al were co-precipitated under ultrasonic radiation in basic medium.
- Spinel $CoAl_2O_4$ and/or Co_3O_4 structure was detected for Co–Al mixed oxide, while gamma Al_2O_3 and Mn_3O_4 species were detected in Mn–Al mixed oxides.
- Acetone was the main formed product on using both oxides, in which they combined the dehydrogenating metal sites and the acid–base properties of the oxide required for the dehydrogenation/condensation/ketonization pathways for acetone formation.
- Ethylene is formed at higher reaction temperature (400–500 °C) on using Co–Al mixed oxide.
- The narrow pore structure and reaction conditions may afford the active sites for ethylene formation.

N.B., thus this work offered the low-cost prepared nano-sized mixed oxide materials bearing acid–base properties; in other words, the prepared nano-sized Co–Al and Mn–Al metal oxide materials can have a high activity either at lower or higher reaction temperature towards the ethanol conversion to produce acetone and/or ethylene.

References

1. Nakajima, T., Nameta, H., Mishima, S., Matsuzaki, I., Tanabe, K.: A highly active and highly selective oxide catalyst for the conversion of ethanol to acetone in the presence of water vapour. J. Mater. Chem. **4**, 853–858 (1994)
2. Yee, A., Morrison, S., Idriss, H.: A study of the reactions of ethanol on CeO2 andPd/CeO2 by steady state reactions, temperature programmed desorption, and in situ FT-IR. J. Catal. **186**, 279–295 (1999)
3. Nakajima, T., Tanabe, K., Yamaguchi, T., Matsuzake, I., Mishima, S.: Conversion of ethanol to acetone over zinc oxide–calcium oxide catalyst : optimization of catalyst preparation and reaction conditions and deduction of reaction mechanism. Appl. Catal. A. Gen. **52**, 237–248 (1989)
4. Karim, A., Su, Y., Sun, J., Yang, C., Strohm, J., King, D., Wang, Y.: A comparative study between Co and Rh for steam reforming of ethanol. Appl. Catal. B **96**, 441–448 (2010)
5. Ni, M., Leung, D., Leung, M.: A review on reforming bio-ethanol for hydrogen production. Int. J. Hydrog. Ene. **32**, 3238–3247 (2007)
6. Nishiguchi, T., Matsumoto, T., Kanai, H., Utani, K., Matsumura, Y., Shen, W., Imamura, S.: Catalytic steam reforming of ethanol to produce hydrogen and acetone. Appl. Catal. A: Gen. **279**, 273–277 (2005)

7. Rybak, P., Tomaszewska, B., Machocki, A., Grzegorczyk, W., Denis, A.: Conversion of ethanol over supported cobalt oxide catalysts. Catal. Today **176**, 14–20 (2011)
8. Sun, J., Karimb, A., Mei, D., Engelhard, M., Bao, X., Wang, Y.: New insights into reaction mechanisms of ethanol steam reforming on Co–ZrO2. Appl. Catal. B: Environ. **162**, 141–148 (2015)
9. Asencios, Y., Sun-Kou, M.: Synthesis of high-surface-area γ-Al2O3 from aluminum scrap and its use for the adsorption of metals: Pb(II), Cd(II) and Zn(II). Appl. Surf. Sci. **258**, 10002–11001 (2012)
10. Song, H., Zhang, L., Ozkan, U.: Effect of synthesis parameters on the catalytic activity of Co–ZrO2 for bio-ethanol steam reforming. Green Chem. **9**, 686–694 (2007)
11. Xu, W., Liu, Z., Johnston-Peck, A., Senanayake, S., Zhou, G., Stacchiola, D., Stach, E., Rodriguez, J.: Steam reforming of ethanol on Ni/CeO2: reaction pathway and interaction between Ni and the CeO2 Support. ACS Catal. **3**, 975–984 (2013)
12. Wang, W., Wang, Y., Liu, Y.: Production of hydrogen by ethanol steam reforming over nickel–metal oxide catalysts prepared via urea–nitrate combustion method. Int. J. Energy Res. **35**, 501–506 (2011)
13. Palomaresa, A., Francha, C., Riberab, A., Abelln, G.: Amorphous features of working catalysts. Catal. Today **191**, 47–51 (2012)
14. Reichle, W.: Synthesis of anionic clay minerals (mixed metal hydroxides, hydrotalcite). Solid State Ion. **22**, 135–141 (1986)
15. Chang, Q., Zhu, L., Luo, Z., Lei, M., Zhang, S., Tang, H.: Sono-assisted preparation of magnetic magnesium–aluminum layered double hydroxides and their application for removing fluoride. Ultrason. Sonochem. **18**, 553–561 (2011)
16. Jiang, J., Yu, J., Cheng, T., Xiao, M., Jones, Z., Hao, P., Edwards, Z.: Catalytic combustion of methane over mixed oxides derived from Co–Mg/Al ternary hydrotalcites. Fuel Process. Technol. **91**, 97–102 (2010)
17. Wang, S., Wang, W., Zuo, J., Qian, Y.: Electrodeposition and characterization of Fe doped CdSe thin films from aqueous solution. Mater. Chem. Phys. **68**, 246–251 (2001)
18. Choudhury, H., Choudhary, A., Sivakumar, M., Moholkar, V.: Mechanistic investigation of the sonochemical synthesis of zinc ferrite. Ultrason. Sonochem. **20**, 294–302 (2013)
19. Goswami, P., Choudhury, H., Chakma, S., Moholkar, V.: Sono-chemical synthesis and characterization of manganese ferrite nanoparticles. Ind. Eng. Chem. Res. **52**, 17848–17855 (2013)
20. Xu, Z., Zeng, H.: Decomposition processes of organic-anion-pillared clays CoaMgbAl(OH)c(TA)d·nH2O. J. Phys. Chem. B **104**, 10206–10214 (2000)
21. Chmielarz, L., Kustrowski, P., Rafalska-Lasocha, A., Dziembaj, R.: Influence of Cu, Co and Ni cations incorporated in brucite-type layers on thermal behaviour of hydrotalcites and reducibility of the derived mixed oxide systems. Thermochim. Acta **395**, 225–236 (2002)
22. Xu, B., Smith, P.: Dehydration kinetics of boehmite in the temperature range 723–873 °K. Thermochim. Acta **531**, 46–53 (2012)
23. Gregg, S., Sing, K.: Adsorption, Surface Area and Porosity, 2nd edn, p. 165. Academic Press, London (1982)
24. Nasikin, M., Wahid, A.: Effect of ultrasonic during preparation on Cu-based catalyst performance for hydrogenation of Co2 to methanol. ASEAN J. Chem. Eng. **5**, 111–115 (2005)
25. Pereza, A., Lamonierb, O., Giraudonb, J., Molinaa, R., Morenoa, S.: Catalytic activity of Co–Mg mixed oxides in the VOC oxidation: effects of ultrasonic assisted in the synthesis. Catal. Today **176**, 286–291 (2011)
26. Gabrovskaa, M., Edreva-Kardjieva, R., Tencheva, K., Tzvetkovb, P., Spojakinaa, A., Petrovc, L.: Effect of Co-content on the structure and activity of Co–Al hydrotalcite-like materials as catalyst precursors for CO oxidation. Appl. Catal. A: Gen. **399**, 242–251 (2011)
27. Rodrigues, C., Zonetti, P., Silva, C., Gaspar, A., Appel, L.: Chemicals from ethanol—The acetone one-pot synthesis. Appl. Catal. A:Gen. **458**, 111–118 (2013)
28. Khassin, A., Yurieva, T., Kaichev, V., Bukhtiyarov, V., Budneva, A., Paukshtis, E., Parmon, V.: Metal–support interactions in cobalt-aluminum co-precipitated catalysts: XPS and CO adsorption studies. J. Mol. Catal. A: Chem. **175**, 189–204 (2001)
29. Laosiripojana, N., Assabumrungrat, S.: Methane steam reforming over Ni/Ce–ZrO2 catalyst: influences of Ce–ZrO2 support on reactivity, resistance toward carbon formation, and intrinsic reaction kinetics. Appl. Catal., A: Gen. **290**, 200–211 (2005)
30. Song, H., Ozkan, U.: Ethanol steam reforming over Co-based catalysts: role of oxygen mobility. J. Catal. **261**, 66–74 (2009)